Probing Specificity of Protein-Protein Interactions with Chiral Plasmonic Nanostructures

Marion Rodier[1], Chantal Keijzer[1,2], Joel Milner[2], Affar S. Karimullah[1], Laurence D. Barron[1], Nikolaj Gadegaard[3], Adrian J. Lapthorn[1*] and Malcolm Kadodwala[1*]

[1]School of Chemistry, Joseph Black Building, University of Glasgow, Glasgow, G12 8QQ

[2]Institute of Molecular, Cell and Systems Biology, University of Glasgow, G12 8TAF

[3]School of Engineering, Rankine Building, University of Glasgow, Glasgow, G12 8LT, UK.

Abstract

Protein-protein interactions (PPIs) play a pivotal role in many biological processes. Discriminating functionally important well-defined protein-protein complexes formed by specific interactions from random aggregates produced by non-specific interactions is therefore a critical capability. While there are many techniques which enable rapid screening of binding affinities in PPIs, there is no generic spectroscopic phenomenon which provides rapid characterisation of the structure of protein-protein complexes. In this study we show that chiral plasmonic fields probe the structural order and hence the level of PPI specificity in a model antibody-antigen system. Using surface immobilised Fab' fragments of polyclonal rabbit IgG antibodies with high specificity for bovine serum albumin (BSA), we show that chiral plasmonic fields can discriminate between structurally anisotropic ensemble of BSA-Fab' complexes and random ovalbumin (OVA)-Fab' aggregates, demonstrating their potential as the basis of a useful proteomic technology for the initial rapid high-throughput screening of PPIs.

TOC Graphic

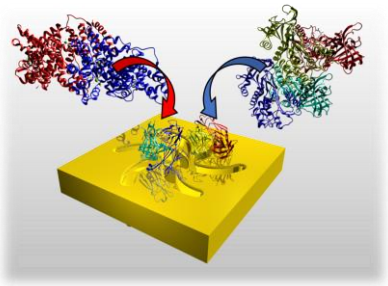

Protein-protein interactions (PPIs) are ubiquitous players in biological processes. Functionally important PPIs involve specific interactions between two or more proteins resulting in a structurally well-defined complex. Non-specific PPIs produce random aggregates which have no biological function[1]. Detecting and characterising PPIs and discriminating between functionally relevant specific and non-specific interactions is a fundamental problem in proteomics and has broader implications in areas such as immunology, medical diagnostics and biosensing. The prerequisite signature of a specific PPI is the formation of a well-defined complex. Consequently, structural probes such as protein crystallography[2] and NMR[3] provide an unambiguous characterisation of the specificity of a PPI. These approaches are complex, labour intensive and time consuming. Unfortunately, spectroscopic techniques, such as circular dichroism (CD)[4] used for routine rapid low-resolution characterisation of biomolecular secondary structure are ineffective at characterising the higher order structure of a protein-protein complex. Hence, techniques for rapid routine assaying of PPI, such as surface plasmon resonance (SPR), isothermal titration calorimetry (ITC) and enzyme-linked immunosorbent assay (ELISA), rely on using the strength (*i.e.* selectivity) of the binding in a protein-protein complex to parameterise the nature of the PPI. Binding affinity strength is a more qualitative means of parametrising the specificity of a PPI compared to direct structural characterisation of protein-protein complexes[5].

In this paper, a fundamentally new spectroscopic method for studying the nature of protein-protein complexes is presented. Chiral near fields created by the optical excitation of chiral plasmonic structures are used to detect the level of structural order within a protein-protein complex. As an exemplar system we studied complexes based on a Fab' fragment of the polyclonal rabbit IgG antibody, that demonstrates high specificity for bovine serum albumin (BSA) and little or no cross-reactivity to other serum proteins. Structural distortions in the Fab' fragment induced by immobilisation on an Au surface results in a loss of selectivity. Consequently, the Fab' fragment can now form complexes with either BSA or ovalbumin (OVA), with the latter binding in a less-specific manner than the former. The chiroptical properties of the chiral plasmonic structures are modified by the presence of a chiral dielectric (protein) layer. Changes in chiroptical properties induced by the chiral layers are asymmetric between left and right-handed structures[6-8]. The magnitude of the asymmetry is dependent on the structural order of the chiral medium, with structurally anisotropic (*i.e.* ordered) media producing larger asymmetries than equivalent isotropic ones. Consequently, the level of structural order of a protein-protein complex can be used to discriminate between specific and non-specific PPIs. As a direct structural probe, chiral plasmonic fields provide a more incisive route than existing techniques for the rapid low-resolution characterisation of PPIs, thus providing a powerful new technique for the biophysical toolbox.

Substrate and asymmetry parameters

This study utilises Au metafilms templated on to nanostructured polycarbonate substrates. The metafilms are ~100 nm thick and consist of "Shuriken" shaped indentations, **figure 1**, with either left (LH) or right-handed (RH) six-fold rotational symmetry arranged in a square lattice. For brevity these substrates are referred to as "template plasmonic substrates" (TPS)[9]. The nanoscopic indentations in the surface polycarbonate substrate have a depth of ~80 nm, are 500 nm in diameter from arm to arm, and have a pitch of 700 nm. The chiral and optical properties of these substrates are discussed in detail elsewhere[9-10]. Reflectance and optical rotatory dispersion (ORD) spectra collected from LH and RH TPSs immersed in buffer are shown in **figure 2**. The ORD spectra display a bisignate line shape, which as expected switches sign between LH and RH structures. Similar reflectance spectra are obtained for LH and RH structures, and they display a region of enhanced reflectivity. Such behaviour has been observed in previous studies and is referred to as plasmonic induced transparency / reflectivity (PIT/PIR) depending on the measurement. The premise of the reported measurements is that structurally anisotropic ordered protein–protein complexes produce larger asymmetries between the optical properties of LH and RH structures than disordered structurally isotropic ones[6-7, 10-11]. Consequently, by monitoring the level of asymmetry between optical properties information on the structural anisotropy of the protein-protein complex can be inferred. The asymmetries between ORD spectra for LH and RH structures are parameterised using a factor based on the peak-to-peak heights of the bisignate lines shapes. Specifically, the ORD asymmetry is parameterised using

$$\frac{PP_{LH\,(RH)}^{Protein}}{PP_{LH\,(RH)}^{Buffer}} = I_{LH(RH)} \qquad \textbf{(1)}$$

where $PP_{LH\,(RH)}^{Buffer}$ and $PP_{LH\,(RH)}^{Protein}$ are the peak-to-peak heights of bisignate resonance for LH (RH) substrates in buffer and with immobilised protein. From this the following protein induced asymmetries between LH and RH substrates can be parameterised by:

$$\frac{I_{RH}}{I_{LH}} = A \qquad \textbf{(2)}$$

where A = 1 indicates an absence of asymmetry. The greater the deviation of A from 1, the larger the asymmetry. In the case of protein –protein complexes the A parameter is derived from the spectrum of the individual protein before binding rather than from that of the buffer.

The asymmetry parameter for the reflectance spectra is derived from a term, ϕ, extracted from fitting the PIR line shape using a phenomenological model (see supplementary information). The values of

changes in values of ϕ for LH and RH structures, $\Delta\phi_{LH/RH}$ induced by a binding event are used to derive an asymmetry parameter:

$$\Delta\Delta\phi = \Delta\phi_{RH} - \Delta\phi_{LH}$$

The larger the magnitude of $\Delta\Delta\phi$ the greater the asymmetry between reflectance spectra. Absorption of biomaterials onto any plasmonic material cause the plasmonic resonances to red shift due to an increase in the local refractive index, the level of the shift being proportional to the thickness of the layer[12]. Hence, in the case of the TPS the amount of material adsorbed can be parametrised using the average wavelength shift ($\Delta\lambda_{Av}$) of the bisignate ORD of LH and RH TPS.

Theory and Modelling

The proposition that *A* and $\Delta\Delta\phi$ can be used to parameterise structural (anisotropy) order can be validated using electromagnetic (EM) numerical simulations. The influence of a chiral molecular (dielectric) medium on the (chir)optical properties of a plasmonic nanostructure is derived from the following constitutive relationships:

$$\boldsymbol{D} = \varepsilon_o \varepsilon_r \boldsymbol{E} + i\xi \boldsymbol{B} \qquad \textbf{(3)}$$

$$\boldsymbol{H} = \boldsymbol{B}/\mu_0\mu_r + i\xi \boldsymbol{E} \qquad \textbf{(4)}$$

Here, ε_o is the permittivity of free space, ε_r is the relative permittivity, μ_0 is the permeability of free space, μ_r is the relative permeability, $\boldsymbol{E}$ is the complex electric field, $\boldsymbol{B}$ is the complex magnetic flux density, $\boldsymbol{H}$ is the magnetic field, $\boldsymbol{D}$ is the electric displacement field and ξ is a second rank tensor describing the chiral property of a molecular layer. ξ is only non-zero for a chiral dielectric. The sign of the pseudoscalar tensor elements ξ_{ij} (*i, j = x, y &* z) is defined by the handedness of the chiral dielectric. For an isotropic chiral medium only electric-dipole – magnetic dipole interactions contribute significantly to the asymmetry in optical responses. In this case only the diagonal elements of the chirality tensor, ξ are non-zero, with:

$$\xi = \begin{bmatrix} \xi_{xx} & 0 & 0 \\ 0 & \xi_{yy} & 0 \\ 0 & 0 & \xi_{zz} \end{bmatrix} \qquad \textbf{(5)}$$

For a structurally isotropic chiral medium then

$$\xi_{xx}^{iso} = \xi_{yy}^{iso} = \xi_{zz}^{iso} \qquad \textbf{(6)}$$

While for anisotropic media

$$\xi_{zz}^{ani} \gg \xi_{yy}^{ani} = \xi_{xx}^{ani} \qquad \textbf{(7)}$$

The diagonal elements for isotropic and anisotropic tensors are related by:

$$\xi_{xx}^{iso} = \frac{1}{3}\left[2\xi_{xx}^{ani} + \xi_{zz}^{ani}\right] \qquad \textbf{(8)}$$

The differences in the chiral response of isotropic and anisotropic expressed in equations (6)-(8) are responsible for enhanced CD from protein oriented in membrane (lipid) layers[13]. From these previous studies it can be estimated that for proteins with CD resonances in the UV, $\frac{\xi_{zz}^{ani}}{\xi_{xx}^{ani}} \gtrsim 10$. Consequently we assign $\xi_{xx}^{iso} = 1.7 \times 10^{-4}$ for isotropic and $\xi_{xx}^{aniso} = 1 \times 10^{-5}$ and $\xi_{zz}^{aniso} = 5 \times 10^{-4}$ for anisotropic chiral media. Using these parameters, the effects of 20 nm thick anisotropic and isotropic protein layers refractive index 1.5 have been simulated, **Figure 3**, where the associate *A* parameters are also given. The simulated ORD spectra deviate slightly from a pure bisignate lineshape, which can be attributed to the modelling underestimating the level of coupling between the dark and bright modes of the nanostructure. This we attribute to structural differences, arising from the fabrication process (*i.e.* sloping sides, surface roughness and symmetry lowering defects), between the actual structure and the idealised form that is modelled. However, the simulations clearly demonstrate that anisotropic chiral media induce significantly larger asymmetries in ORD and reflectance spectra than equivalent isotropic ones.

Fab' Fragment

Polyclonal antibodies are an ensemble of antibodies that can recognise multiple epitopes on an antigen. By contrast, a monoclonal antibody binds uniquely to a single epitope of an antigen and therefore displays greater specificity. In the current study we have immobilised onto the TPS a fragment derived from polyclonal rabbit IgG which has been produced against BSA, referred to as poly anti-BSA IgG [Thermofisher]. The hypothesis we wanted to test was that orientational distributions of the different individual antibody-BSA complexes would have a level of anisotropy, leading to a measurable signal asymmetry. A narrow structural distribution is expected as the mixture of antibodies recognise a relatively small number of epitopes which are not equally immunogenic. An enzyme-linked immunosorbent assay, ELISA was used as a control to confirm that anti-BSA IgG has a

high binding affinity towards BSA (see supplementary information). The effects of adsorption on to gold surfaces on the activity of IgG has been studied[14]. This previous work established that IgG adopts at least four adsorption geometries on Au surfaces. Studies have also shown that immobilising IgG onto Au surfaces significantly degrades its effectiveness[14]. This degradation of performance is attributed to a combination of structural heterogeneity and the large size of IgG facilitating denaturisation on adsorption. To minimise the loss of functionality an approach based on immobilising functional active fragments of IgG has been used[15-16]. Compared to the whole antibody immobilised Fab' fragments adopt more homogenous adsorption structures and are less susceptible to denaturing[17-18]. The IgG is typically treated with a specific protease papain to release smaller 50 kDa antigen-binding fragment (Fab') which is composed of one constant and one variable domain of each of the heavy and the light chains of the IgG. The IgG protein can be broken down into its constituent Fab' fragments (see methods) which have free sulfhydryl's for attachment to the gold surfaces of the TPSs. This produces a consistent attachment point for the poly anti-BSA Fab' fragments which should significantly limit effects due to binding orientation. To minimise the degree to which the Fab' fragment is denatured it is co-adsorbed with a thiol: triethylene glycol mono-11-mecaptoundecyl (EG-thiol)[19]. The EG-thiol is neutral spacer molecule, so any interactions between Fab' molecules and a surface will be minimised[20]. This layer will subsequently be referred to as a mixed Fab' layer. ORD and reflectance spectra collected from the LH and RH structures with mixed Fab' layers are displayed in **Figure 2** with corresponding *A*, $\Delta\Delta\varphi$ and $\Delta\lambda_{AV}$ values given in **table 1**. For comparison Fab' layers without EG-thiol spacers, formed from buffered solutions with concentrations of 10 and 100 μg / ml have been studied (see supplementary information for spectra). The principle conclusions from these data are: there was no significant difference in the amount of Fab' adsorbed from the two solutions; and the observed levels of asymmetries (as parameterised by *A* and $\Delta\varphi$) were lower in the absence of the spacer. This last point is consistent with the expected behaviour, specifically that the presence of the EG-thiol reduces the level of structural perturbation of the absorbed Fab'.

***BSA + Fab'*: Reflectance and ORD spectra**

To demonstrate the ability of chiral plasmonic fields to discriminate between specific and non-specific PPIs we compared the behaviour of polyclonal Fab' with the antigen BSA and a non-antigen OVA. This is a protein found in egg white, which is widely used in immunology[21]. OVA has 385 amino acid residues and a Serpin fold which has a mix of α-helix and β-sheet structure forming a dimer in solution. BSA has 583 amino acids, has an Albumin fold which is predominantly α-helix and is a monomer in solution. Both proteins are readily available, stable and have a similar isoelectric points of 5.2 and 4.7 respectively. Mixed Fab' functionalised TPSs were exposed to both BSA (0.1 and 1 $mgml^{-1}$) and OVA (1

mgml^{-1}); and for comparison BSA was adsorbed on to an unfunctionalised TPS. ORD and reflectivity data for the three sets of experiments are shown in **Figure 4-6**, with corresponding *A*, $\Delta\Delta\varphi$ and $\Delta\lambda_{AV}$ values given in **table 2**. The $\Delta\lambda_{AV}$ data clearly shows that both BSA and OVA bind to the mixed Fab' layer. The $\Delta\lambda_{AV}$ values of 1.0 and 0.6 nm scale with the molecular mass of the BSA (66.4 kDa) and OVA (42.7 kDa) monomers (*i.e.* the ratios of $\Delta\lambda_{AV}$ and monomer molecular mass are equal $\sim$ 0.6) which means that equal amounts of the two proteins are adsorbed. In addition, as would be expected with the presence of the bio-repellent spacer layer, less BSA adsorbs, ~55%, on to the mixed layer compared to the bare surface. This data clearly demonstrates that both BSA and OVA bind strongly to the anti-BSA Fab' since they are retained on the surface even after rinsing in the presence of PBS buffer. An ELISA was used to confirm that there is no specific binding of OVA to the polyclonal rabbit IgG antibody in solution (see supplementary information). Although, similar quantities of BSA and OVA adsorb, different levels of asymmetries are observed for each, with a significant asymmetry observed for BSA but not OVA. This suggests that while BSA binds specifically to the ensemble of anti BSA Fab' molecules on the surface producing a significant asymmetry, OVA is binding non-specifically to the same ensemble producing almost no asymmetry. So, despite the precautions taken to minimise structural distortions, the selectivity of the Fab' proteins have in part been affected by immobilisation directly onto the Au surface of TPS, thus enabling OVA to bind. This degrading of selectivity has been observed in SPR measurements in which such antibodies / antibody fragments are immobilised on to an unstructured Au films[17]. The loss of selectivity can be attributed to a structural distortion of the Fab' fragment which generates protein surfaces that results in non-specific binding of OVA. Since no specific epitiopes on the surface of the OVA are involved in binding random Fab'-OVA aggregates are formed which on average for the ensemble have an isotropic chiral dielectric response. In this way we are able to discriminate between specific and non-specific binding partners. It should be pointed out that in the absence of the Fab' fragment a 100% EG-thiol SAM inhibits the adsorption of proteins onto the TPS surface[22]. Thus any BSA and OVA retained on the surface must be bound to the Fab' fragment.

In summary, we show that spectroscopic measurements utilising chiral plasmonic nanostructures provide a description of the specificity of a PPI based on the level of structural anisotropy of the complex. The strategy is unique in that it is rapid and provides a structural based measure of specificity. These capabilities contrast with established state-of-the-art strategies based on measuring the strength of binding affinities, which monitor selectivity in binding rather than the specificity of the PPI. This additional structural component to the parameter space of the measurement provides a mechanism for rapid screening of PPIs. A capability ideal for medical diagnostic or proteomic applications where high-throughput approaches are a prerequisite.

ACKNOWLEDGEMENTS

The authors acknowledge financial support from the Engineering and Physical Sciences Research Council (EP/P00086X/1).

Supporting Information Available: Experimental Methods (Fabrication of TPS, Optical spectra measurements, Numerical Simulations, Fab' Production, Formation of mixed Fab' layers, Protein binding to mixed Fab' layers); Fitting model and fits to data; BSA ELISA, Simulated reflectance data.

REFERENCES

(1) Jones, S.; Thornton, J. M., Principles of Protein-Protein Interactions. *Proc. Natl. Acad. Sci. U. S. A.* **1996**, *93*, 13-20.
(2) Kobe, B.; Guncar, G.; Buchholz, R.; Huber, T.; Maco, B.; Cowieson, N.; Martin, J. L.; Marfori, M.; Forwood, J. K., Crystallography and Protein-Protein Interactions: Biological Interfaces and Crystal Contacts. *Biochem. Soc. T* **2008**, *36*, 1438-1441.
(3) Zuiderweg, E. R. P., Mapping Protein-Protein Interactions in Solution by NMR Spectroscopy. *Biochemistry* **2002**, *41*, 1-7.
(4) Kelly, S. M.; Price, N. C., The Use of Circular Dichroism in the Investigation of Protein Structure and Function. *Curr. Protein. Pept. Sc.* **2000**, *1*, 349-384.
(5) Berggard, T.; Linse, S.; James, P., Methods for the Detection and Analysis of Protein-Protein Interactions. *Proteomics* **2007**, *7*, 2833-2842.
(6) Kelly, C.; Tullius, R.; Lapthorn, A.; Gadegaard, N.; Cooke, G.; Barron, L. D.; Karimullah, A. S.; Rotello, V. M.; Kadodwala, M., Chiral Plasmonic Fields Probe Structural Order of Biointerfaces. *J. Am. Chem. Soc.* **2018**, 140, 8509-8517.
(7) Tullius, R., et al., Superchiral Plasmonic Phase Sensitivity for Fingerprinting of Protein Interface Structure. *ACS Nano* **2017**, 137, 8380-8383.
(8) Tullius, R.; Karimullah, A. S.; Rodier, M.; Fitzpatrick, B.; Gadegaard, N.; Barron, L. D.; Rotello, V. M.; Cooke, G.; Lapthorn, A.; Kadodwala, M., "Superchiral" Spectroscopy: Detection of Protein Higher Order Hierarchical Structure with Chiral Plasmonic Nanostructures. *J. Am. Chem. Soc.* **2015**, *137*, 8380-8383.
(9) Karimullah, A. S.; Jack, C.; Tullius, R.; Rotello, V. M.; Cooke, G.; Gadegaard, N.; Barron, L. D.; Kadodwala, M., Disposable Plasmonics: Plastic Templated Plasmonic Metamaterials with Tunable Chirality. *Adv. Mater.* **2015**, *27*, 5610-5616.
(10) Kelly, C.; Khorashad, L. K.; Gadegaard, N.; Barron, L. D.; Govorov, A. O.; Karimullah, A. S.; Kadodwala, M., Controlling Metamaterial Transparency with Superchiral Fields. *ACS Photonics* **2018**, *5*, 535-543.
(11) Hendry, E.; Carpy, T.; Johnston, J.; Popland, M.; Mikhaylovskiy, R. V.; Lapthorn, A. J.; Kelly, S. M.; Barron, L. D.; Gadegaard, N.; Kadodwala, M., Ultrasensitive Detection and Characterization of Biomolecules Using Superchiral Fields. *Nat. Nanotechnol.* **2010**, *5*, 783-787.
(12) Anker, J. N.; Hall, W. P.; Lyandres, O.; Shah, N. C.; Zhao, J.; Van Duyne, R. P., Biosensing with Plasmonic Nanosensors. *Nat. Mater.* **2008**, *7*, 442-453.
(13) Burck, J.; Wadhwani, P.; Fanghanel, S.; Ulrich, A. S., Oriented Circular Dichroism: A Method to Characterize Membrane Active Peptides in Oriented Lipid Bilayers. *Acc. Chem. Res.* **2016**, *49*, 184-192.
(14) Trilling, A. K.; Beekwilder, J.; Zuilhof, H., Antibody Orientation on Biosensor Surfaces: A Minireview. *Analyst* **2013**, *138*, 1619-1627.

(15) Albers, W. M.; Auer, S.; Helle, H.; Munter, T.; Vikholm-Lundin, I., Functional Characterisation of Fab '-Fragments Self-Assembled onto Hydrophilic Gold Surfaces. *Colloids Surf., B* **2009**, *68*, 193-199.
(16) Brogan, K. L.; Wolfe, K. N.; Jones, P. A.; Schoenfisch, M. H., Direct Oriented Immobilization of F(Ab ') Antibody Fragments on Gold. *Anal. Chim. Acta.* **2003**, *496*, 73-80.
(17) Crivianu-Gaita, V.; Thompson, M., Immobilization of Fab' Fragments onto Substrate Surfaces: A Survey of Methods and Applications. *Biosens. Bioelectron.* **2015**, *70*, 167-180.
(18) Vikholm-Lundin, I., Immunosensing Based on Site-Directed Immobilization of Antibody Fragments and Polymers That Reduce Nonspecific Binding. *Langmuir* **2005**, *21*, 6473-6477.
(19) Yoshimoto, K.; Nishio, M.; Sugasawa, H.; Nagasaki, Y., Direct Observation of Adsorption-Induced Inactivation of Antibody Fragments Surrounded by Mixed-Peg Layer on a Gold Surface. *J. Am. Chem. Soc.* **2010**, *132*, 7982-7989.
(20) Prime, K. L.; Whitesides, G. M., Adsorption of Proteins onto Surfaces Containing End-Attached Oligo(Ethylene Oxide) - a Model System Using Self-Assembled Monolayers. *J. Am. Chem. Soc.* **1993**, *115*, 10714-10721.
(21) Huntington, J. A.; Stein, P. E., Structure and Properties of Ovalbumin. *J. Chromatogr. B: Biomed. Sci. Appl.* **2001**, *756*, 189-198.
(22) Jack, C., et al., Spatial Control of Chemical Processes on Nanostructures through Nano-Localized Water Heating. *Nat. Commun.* **2016**, *7*.

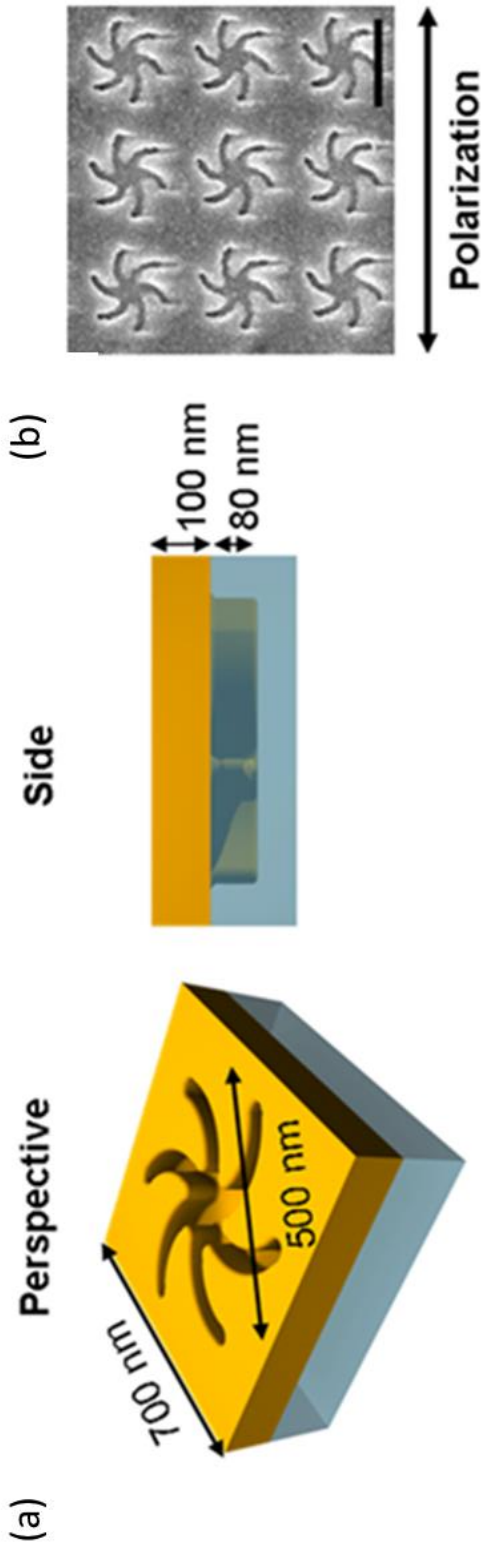

Figure 1. a) A schematic of the shuriken structures; and b) An SEM image of the shuriken structure (scale bar 500 nm), the polarisation direction of incident light used for reflectance and ORD measurement is shown.

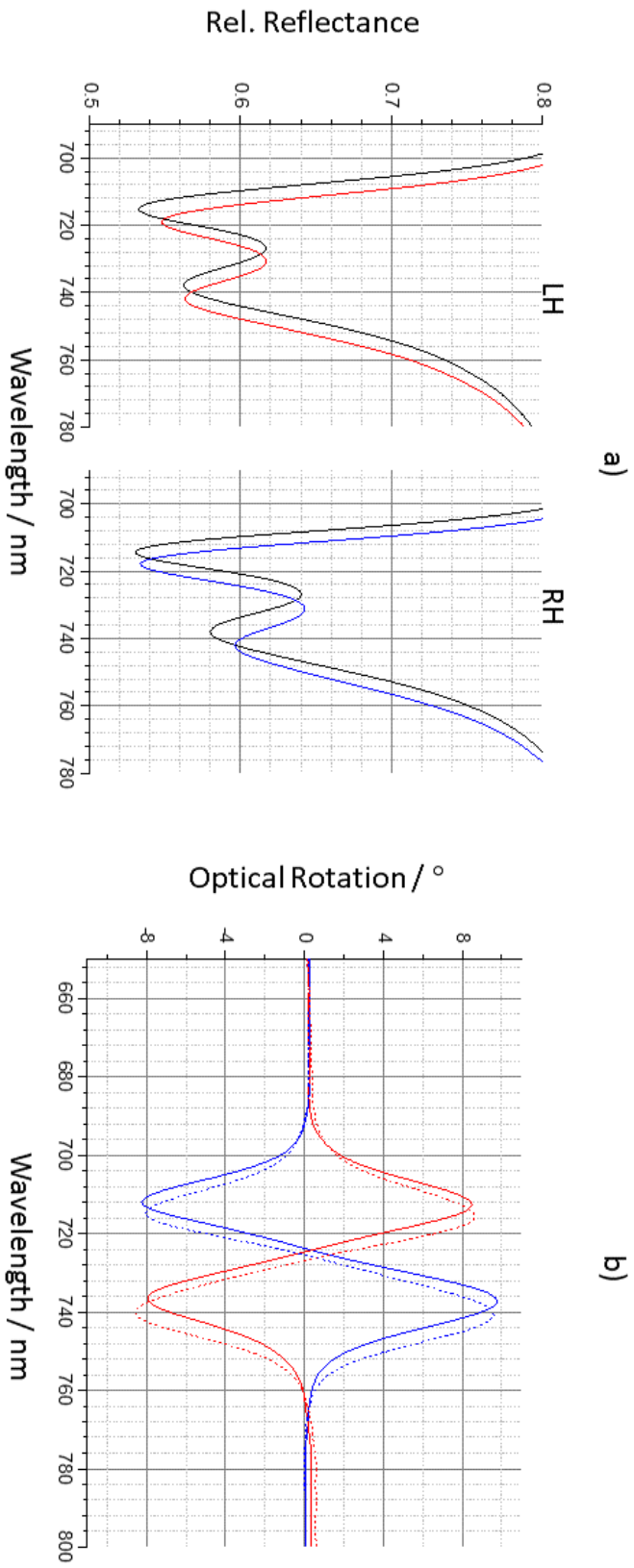

Figure 2. a) Reflectance spectra for LH and RH nanostructures in buffer (black) and in buffer with adsorbed Fab' (LH red and RH blue). b) ORD spectra for LH (red) and RH (blue) nanostructures in the presence of buffer (solid) and buffer and adsorbed Fab' (dashed).

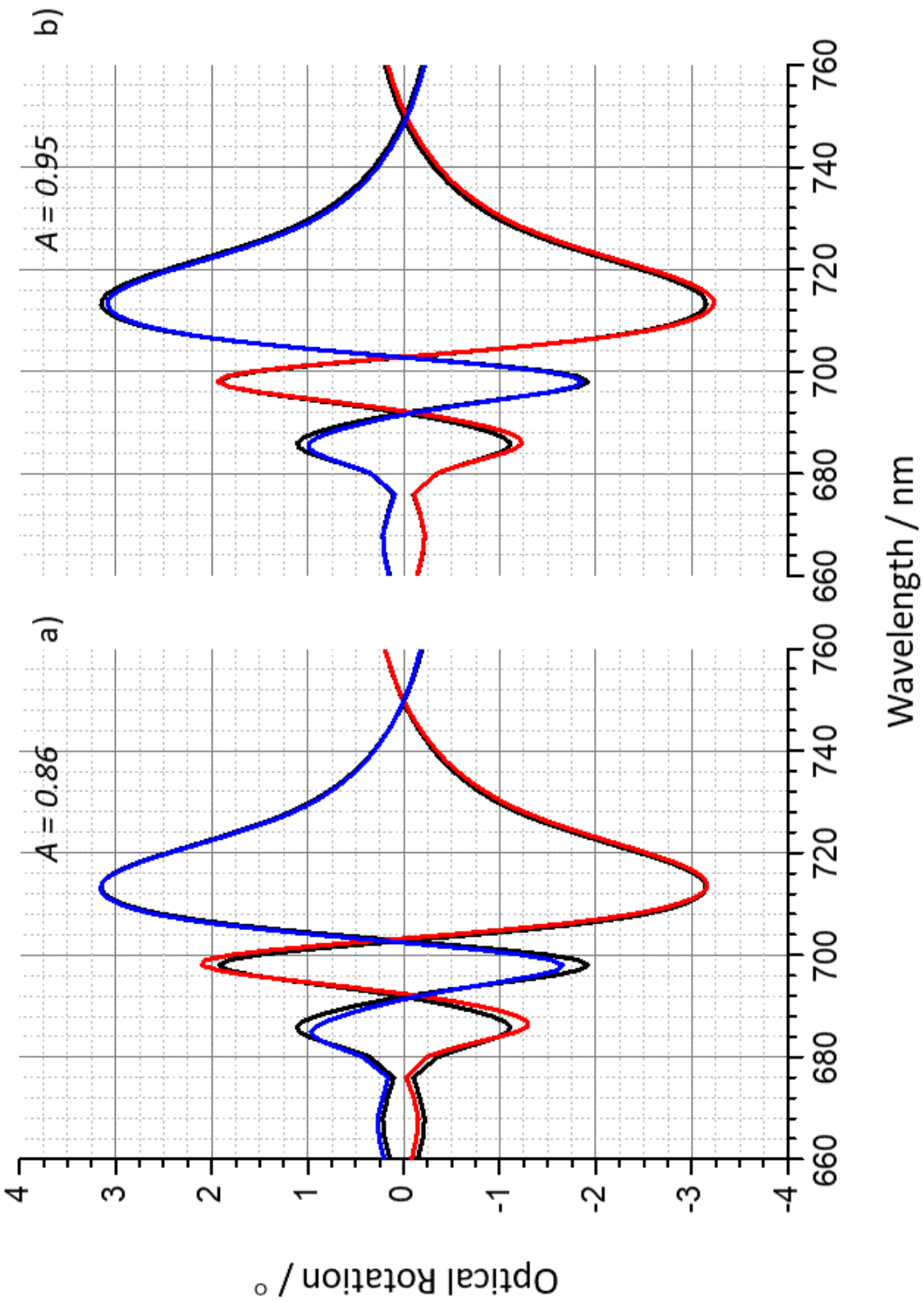

Figure 3. Simulated ORD spectra for a) anisotropic and b) isotropic chiral layers. Red and blue spectra are for left and right-handed structure respectively. The black spectra are provided for comparison and are for achiral dielectric layers. Corresponding reflectance spectra are in supplementary information.

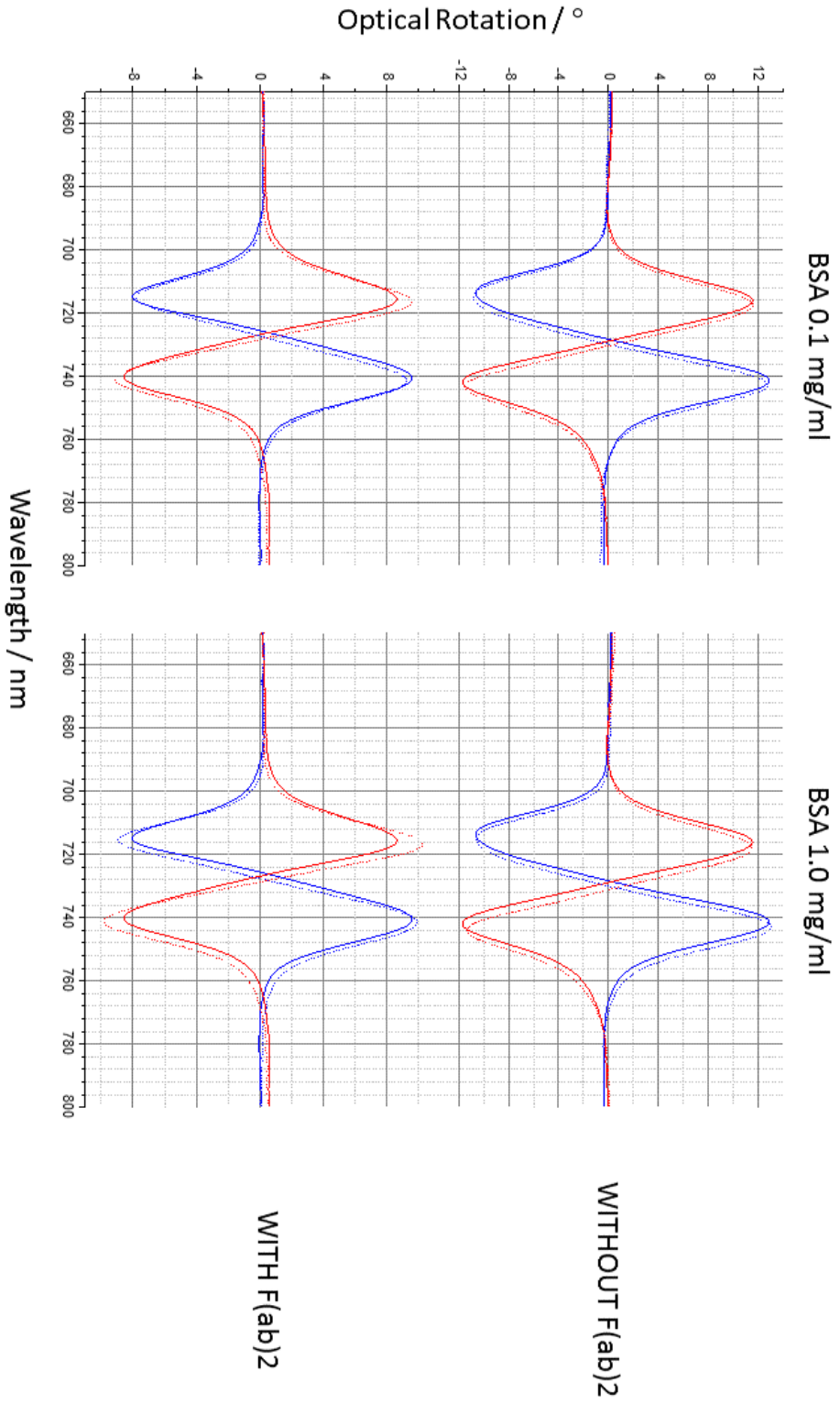

Figure 4, ORD spectra (Red LH, Blue RH) for BSA adsorbed from solution with concentrations of 0.1 and 1 mg / ml onto bare nanostructures (without $F(ab')_2$) and nanostructures covered in the mixed-$F(ab')_2$ layers. Solid and dashed lines represent spectra collected before and after binding of BSA.

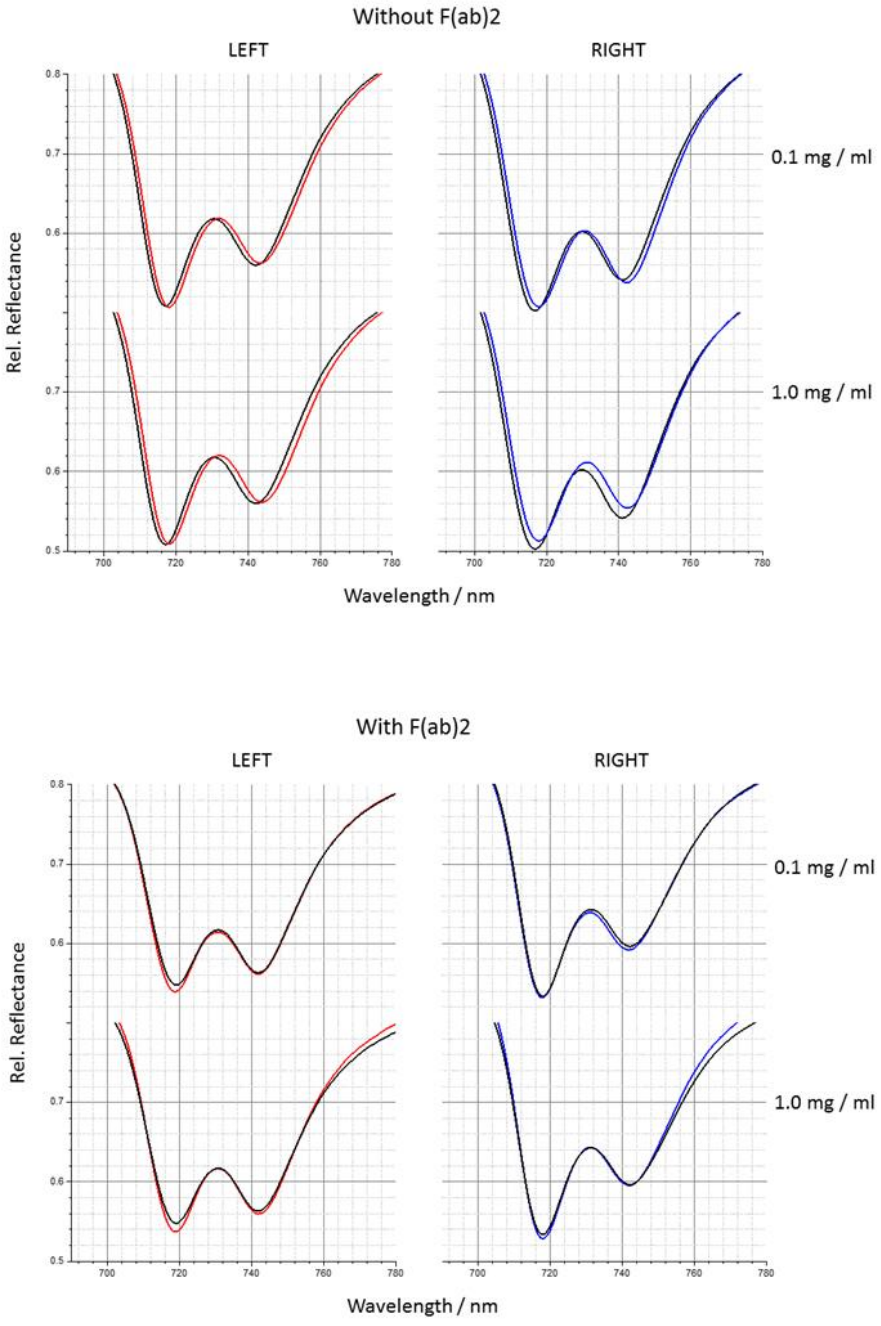

Figure 5. Corresponding reflectance spectra to ORD data presented in Figure4

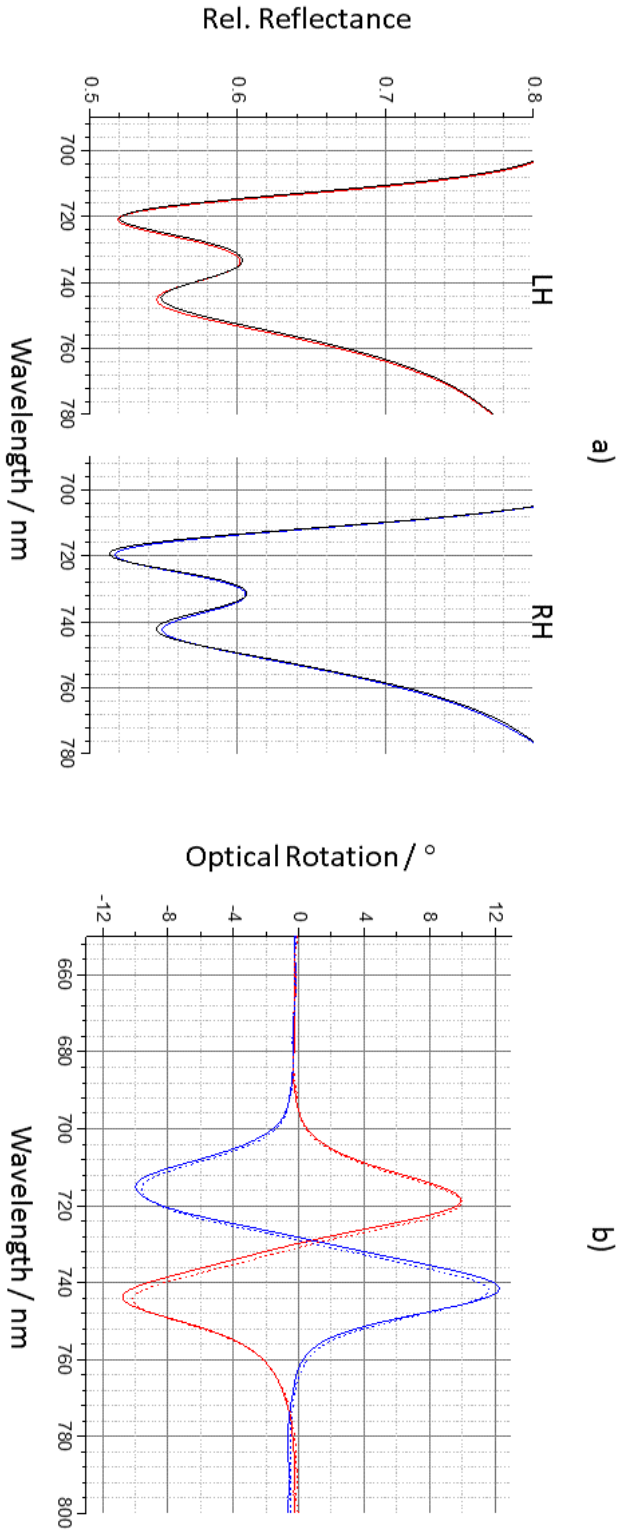

Figure 6. a) Reflectance spectra for LH and RH nanostructures in buffer before (black) and after (red) adsorption of OVA onto mixed-F(ab')$_2$ layers. b) ORD spectra for LH (red) and RH (blue) nanostructures in the presence of buffer before (solid) and after (dashed) adsorption of OVA onto mixed-F(ab')$_2$ layers.

	$F(ab')_2$ 10 µg/mL	$F(ab')_2$ 100 µg/mL	$F(ab')_2$ 10 µg/mL + 0.9mM EG-thiol
$\Delta\lambda_{Av}$	3.00 ± 0.20	3.30 ± 0.20	3.50 ± 0.20
A	1.05 ± 0.02	1.03 ± 0.02	0.92 ± 0.02
$\Delta\Delta\varphi$	-0.70 ± 0.20	-0.60 ± 0.20	- 3.00 ± 0.20

Table 1: optical and fitting parameters extracted from the ORD and the reflectivity spectra for Fab' layers formed under three conditions.

	$F(ab')_2$			No $F(ab')_2$
Protein	BSA		OVA	BSA
Conc. (mg/ml)	0.1	1.0	1.0	1.0
$\Delta\lambda_{Av}$	0.90±0.1	1.0±0.1	0.6±0.1	1.8±0.1
A	0.88±0.02	0.90±0.02	0.98±0.02	1.03±0.02
$\Delta\Delta\varphi$	-2.0±0.2	-2.2±0.2	-0.1±0.2	-0.2±0.2

Table 2: optical and fitting parameters extracted from the ORD and the reflectivity spectra for BSA (0.1 mg/mL and 1 mg/mL) + $F(ab')_2$, OVA (1 mg/mL) + $F(ab')_2$ and BSA (1 mg/mL) on plain gold.